

Fig.1 A schematic diagram of Ni-Cd and Ni-MH cells and the model representation

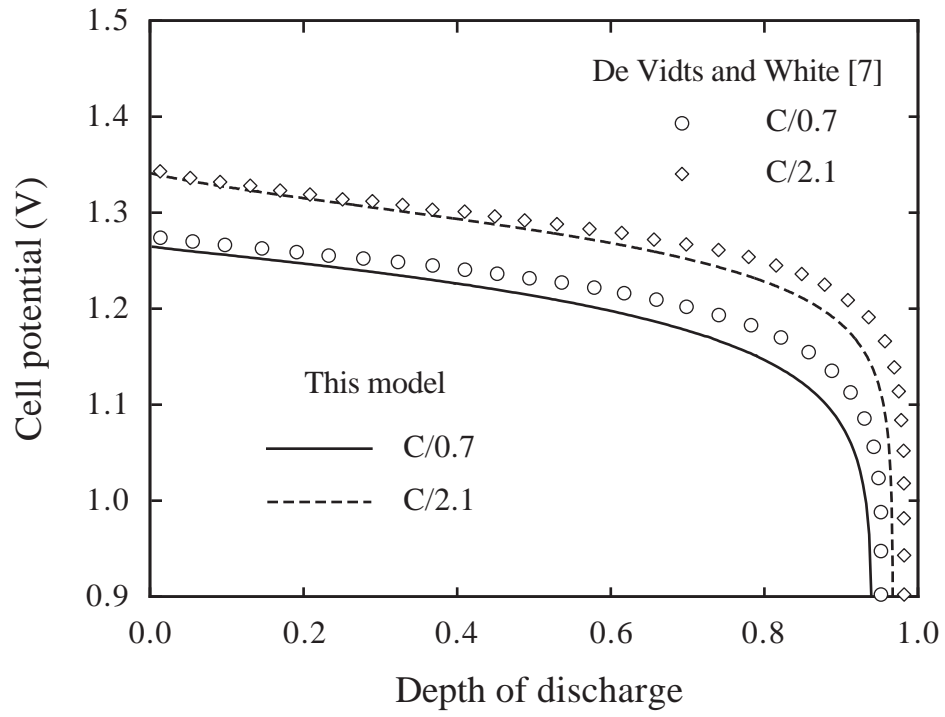


Fig. 2. Predicted Ni-Cd cell potential versus depth of discharge at different discharge rates

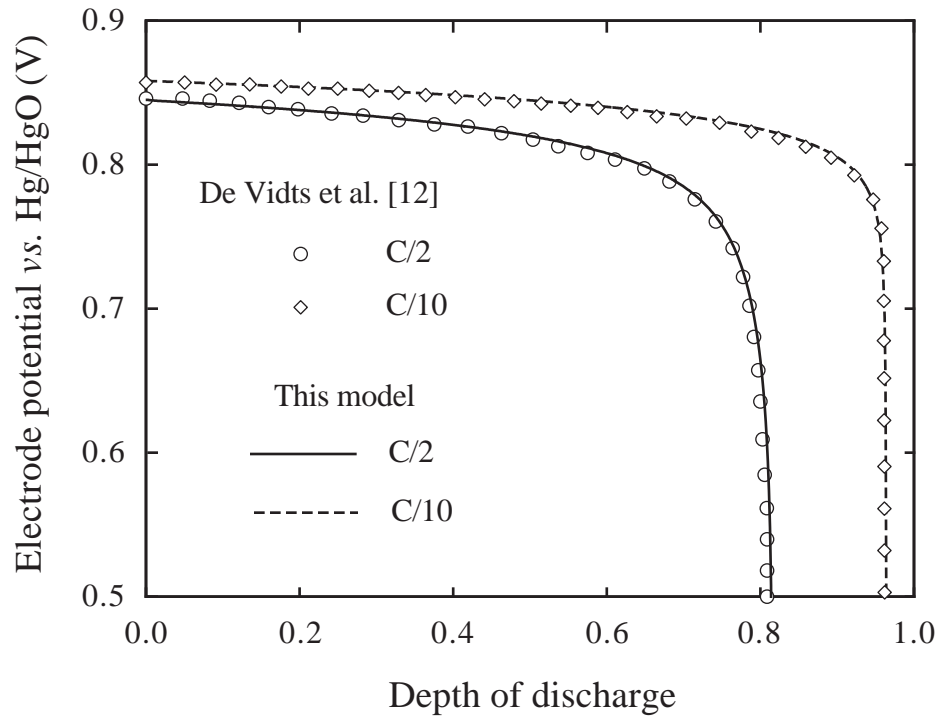


Fig. 3. MH electrode potential versus depth of discharge at different discharge rates

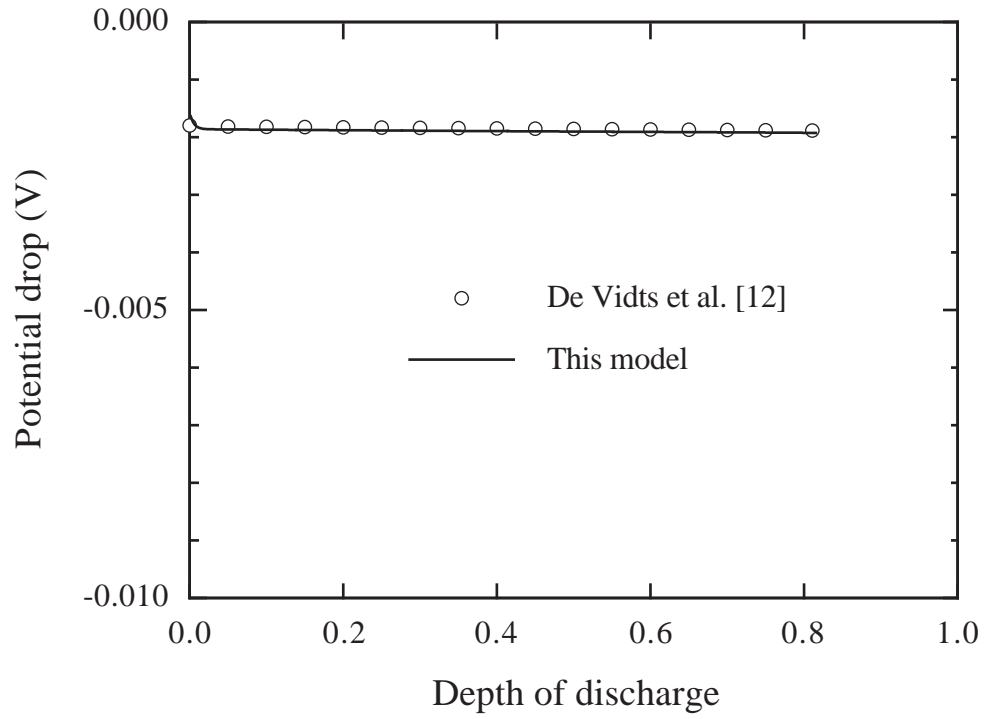


Fig. 4. Potential drop in the electrolyte across the MH electrode as a function of the depth of discharge at the C/2 rate

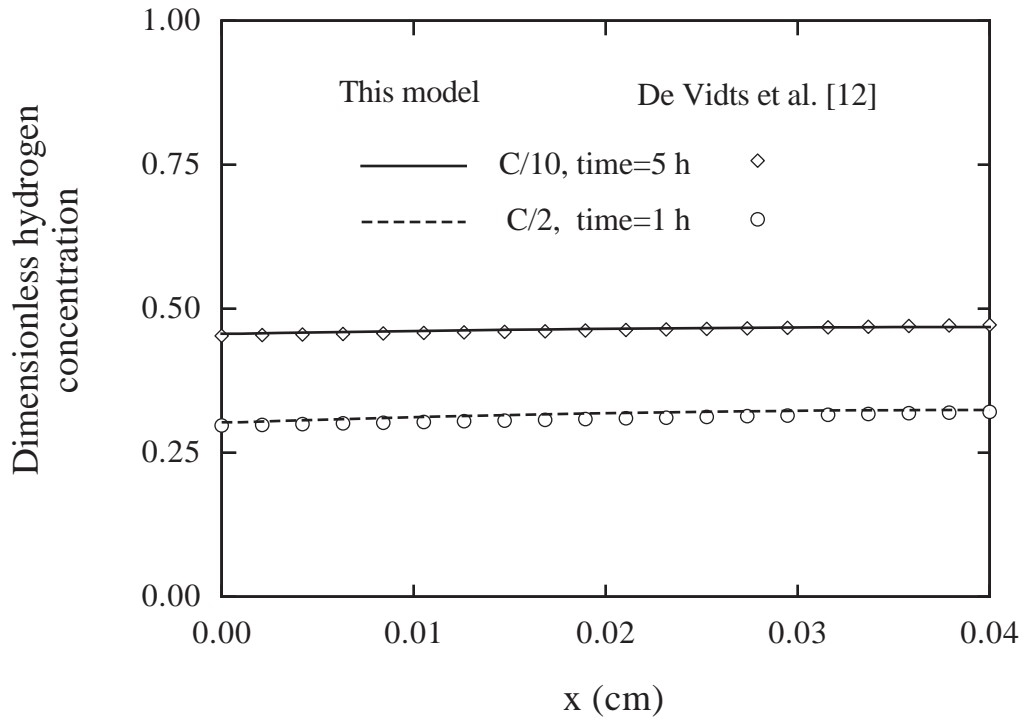


Fig. 5. Representative hydrogen concentration distributions at the MH/KOH interface across the MH electrode in comparison with the results of De Vidts et al. [12]

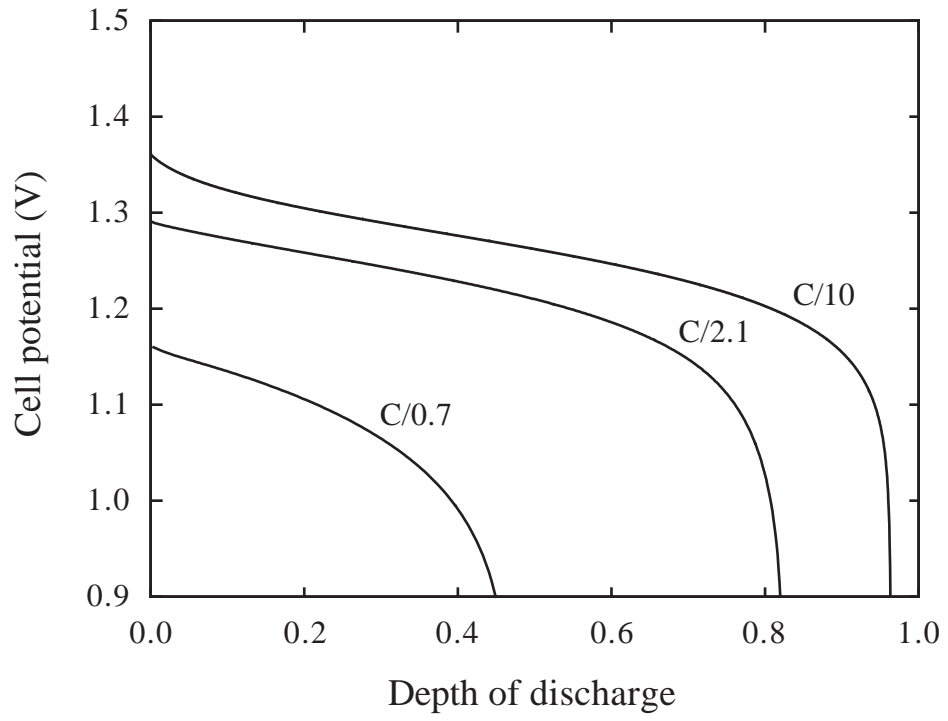


Fig. 6. Predicted Ni-MH cell potential versus depth of discharge at different discharge rates

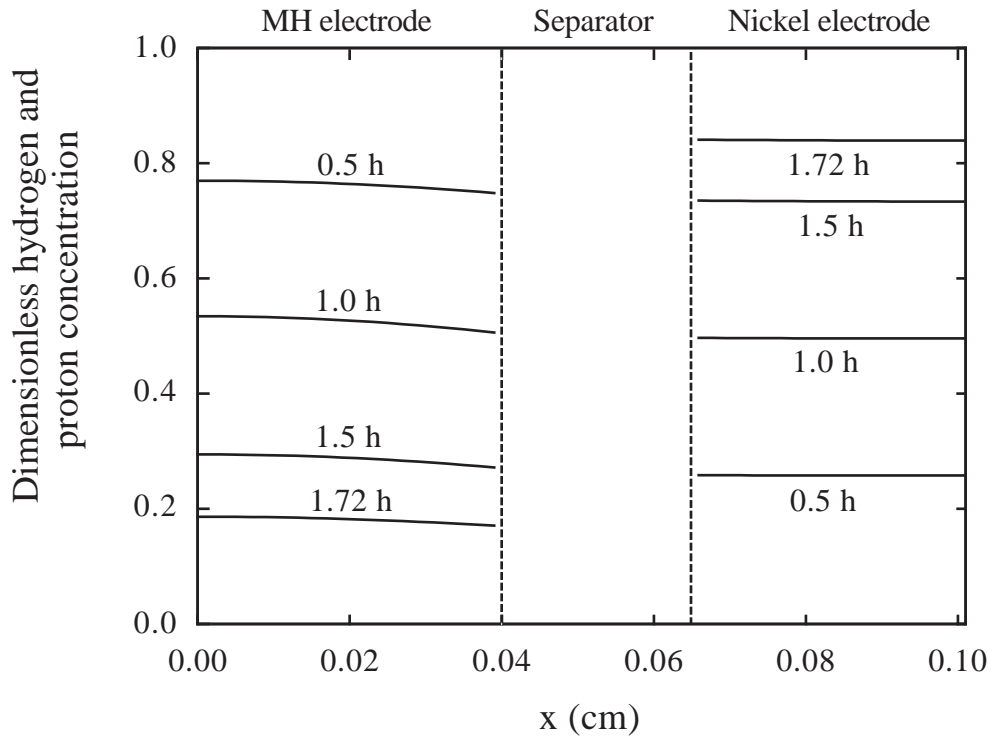


Fig. 7. Profiles of the volume-averaged concentration of hydrogen in the MH electrode and proton in the nickel electrode at various discharge times with the  $C/2.1$  rate

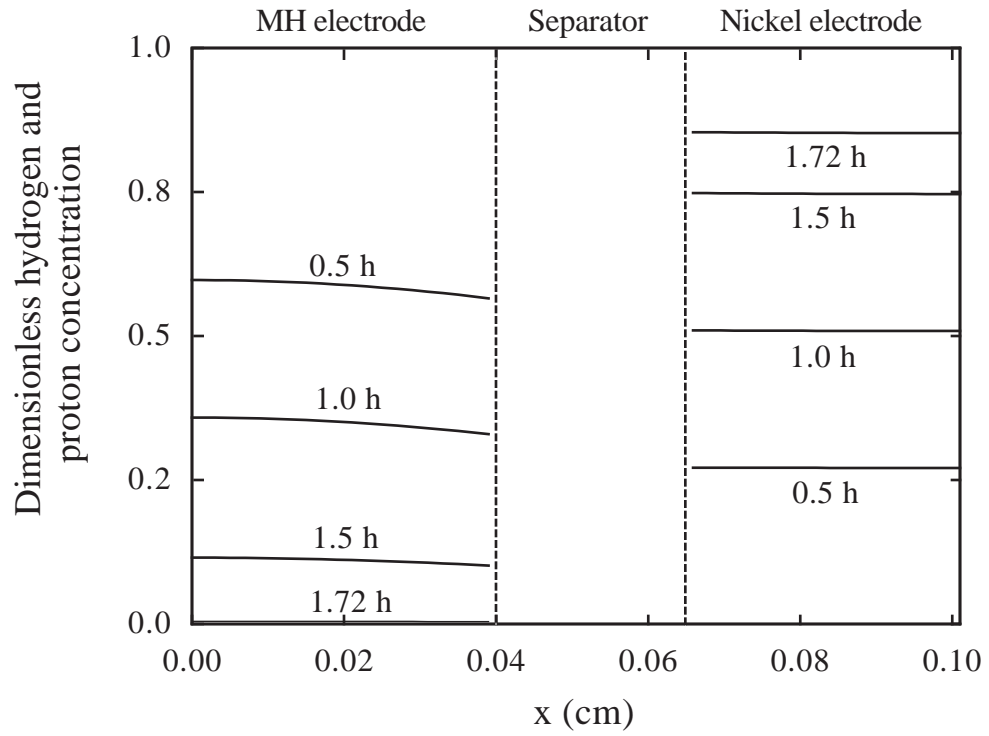


Fig. 8. Profiles of the surface concentration of hydrogen in the MH electrode and proton in the nickel electrode at various discharge times with the  $C/2.1$  rate

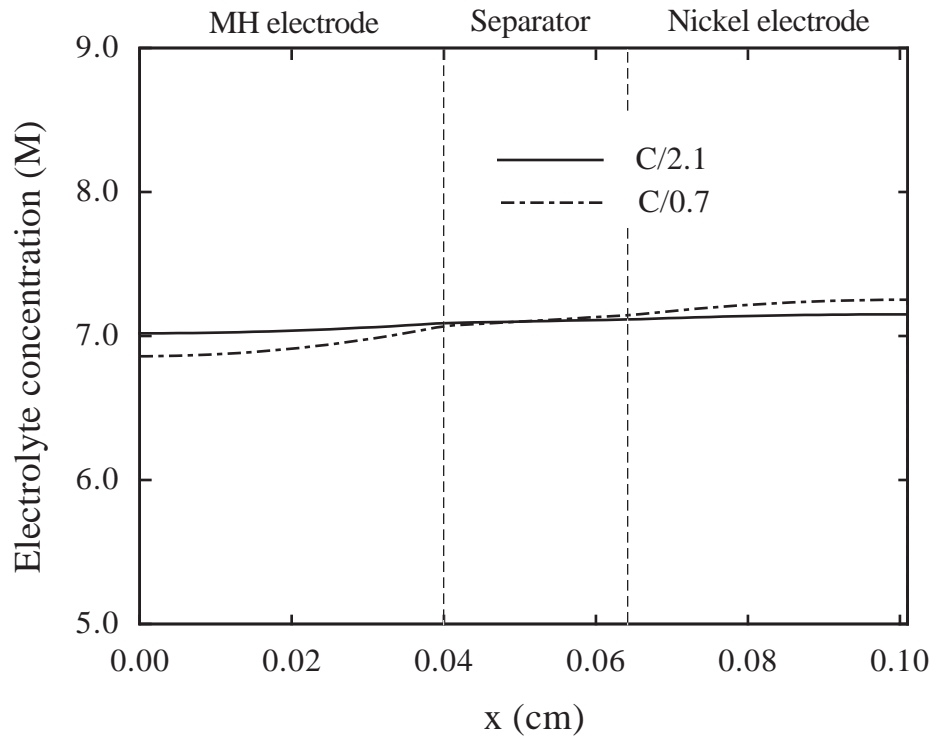
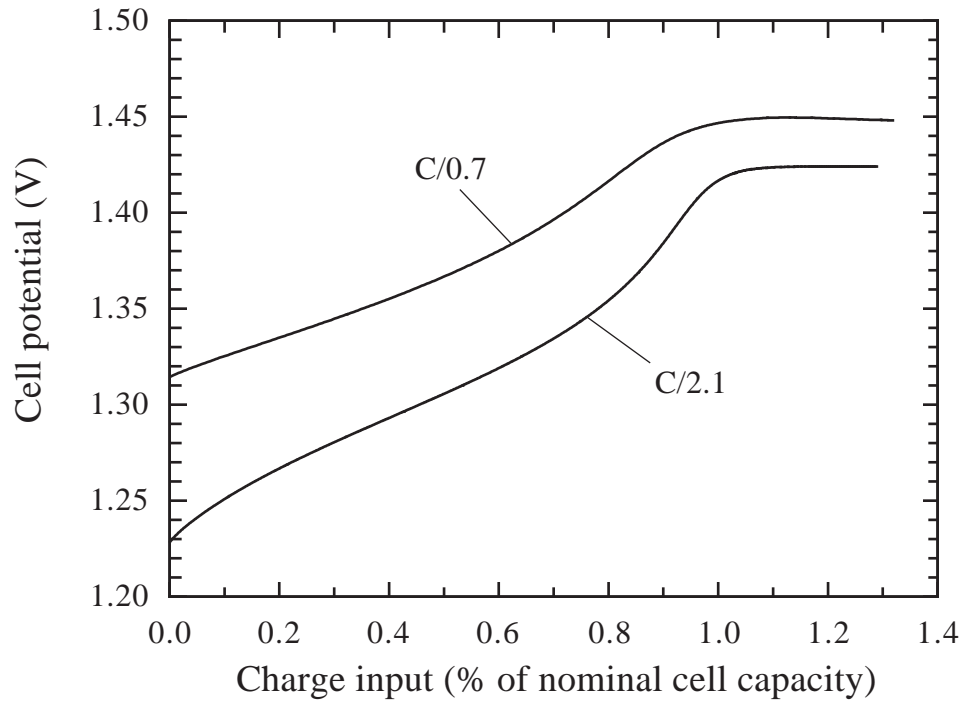
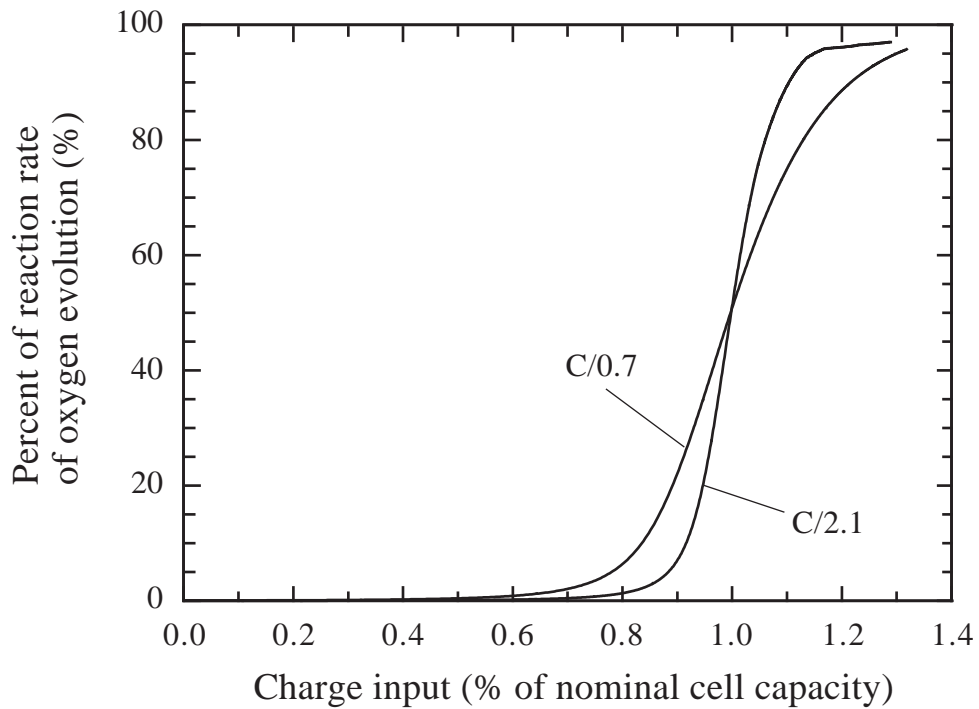


Fig. 9. Predicted electrolyte concentration distributions in the Ni-MH cell at the end of discharge for C/2.1 and C/0.7 rates



(a)



(b)

Fig. 10. Simulation results for the Ni-MH cell during charge and overcharge at different charging rates: (a) cell potential, and (b) percent of the reaction rate of oxygen evolution